Journal of Experimental Botany, Vol. 63, No. 16, pp. 5763–5772, 2012
doi:10.1093/jxb/ers225 Advance Access publication 31 August, 2012
This paper is available online free of all access charges (see http://jxb.oxfordjournals.org/open_access.html for further details)

Journal of Experimental Botany
www.jxb.oxfordjournals.org

RESEARCH PAPER

Atypical iron storage in marine brown algae: a multidisciplinary study of iron transport and storage in *Ectocarpus siliculosus*

Lars H. Böttger[1], Eric P. Miller[2], Christian Andresen[1], Berthold F. Matzanke[1,*], Frithjof C. Küpper[3,†] and Carl J. Carrano[2,*]

[1] Section of Natural Sciences, Isotopes Laboratory, University of Lübeck, Ratzeburger Allee 160, D-23538 Lübeck, Germany
[2] Department of Chemistry and Biochemistry, San Diego State University, San Diego, CA 92182-1030, USA
[3] Microbial and Molecular Biology Department, Scottish Association for Marine Science, Scottish Marine Institute, Oban, Scotland, UK

* To whom correspondence should be addressed. E-mail: carrano@sciences.sdsu.edu or matzanke@isolab.uni-luebeck.de
† Present address: Oceanlab, University of Aberdeen, Main Street, Newburgh AB41 6AA, Scotland, UK.

Received 20 March 2012; Revised 13 July 2012; Accepted 17 July 2012

Abstract

Iron is an essential element for all living organisms due to its ubiquitous role in redox and other enzymes, especially in the context of respiration and photosynthesis. The iron uptake and storage systems of terrestrial/higher plants are now reasonably well understood, with two basic strategies for iron uptake being distinguished: strategy I plants use a mechanism involving induction of Fe(III)-chelate reductase (ferrireductase) and Fe(II) transporter proteins, while strategy II plants utilize high-affinity, iron-specific, binding compounds called phytosiderophores. In contrast, little is known about the corresponding systems in marine, plant-like lineages, particularly those of multicellular algae (seaweeds). Herein the first study of the iron uptake and storage mechanisms in the brown alga *Ectocarpus siliculosus* is reported. Genomic data suggest that *Ectocarpus* may use a strategy I approach. Short-term radio-iron uptake studies verified that iron is taken up by *Ectocarpus* in a time- and concentration-dependent manner consistent with an active transport process. Upon long-term exposure to ^{57}Fe, two metabolites have been identified using a combination of Mössbauer and X-ray absorption spectroscopies. These include an iron–sulphur cluster accounting for ~26% of the total intracellular iron pool and a second component with spectra typical of a polymeric ($Fe^{3+}O_6$) system with parameters similar to the amorphous phosphorus-rich mineral core of bacterial and plant ferritins. This iron metabolite accounts for ~74% of the cellular iron pool and suggests that *Ectocarpus* contains a non-ferritin but mineral-based iron storage pool.

Key words: *Ectocarpus*, iron, marine algae, Mössbauer spectroscopy, storage, transport, X-ray absorbtion spectroscopy.

Introduction

Iron is an essential element for all living organisms due to its ubiquitous role in redox and other enzymes, especially in the context of respiration and photosynthesis. The iron uptake and storage systems of terrestrial/higher plants are now reasonably well understood, with two basic strategies for iron uptake being distinguished: strategy I plants, mainly dicotyledons, use a mechanism involving soil acidification and induction of Fe(III)-chelate reductase (ferrireductase) and Fe(II) transporter proteins (Moog and Bruggemann, 1994; Robinson *et al*., 1999); while strategy II plants (in particular monocotyledons/grasses) have evolved sophisticated systems, similar to those of bacteria and fungi, based on high-affinity, iron-specific, binding compounds called phytosiderophores (Romheld and Marschner, 1986).

In contrast, there is little knowledge about the corresponding systems in marine, plant-like lineages, particularly the multicellular macroalgae (seaweeds). This is important as the iron level in ocean waters is even lower than in most terrestrial environments due both to the low solubility of Fe(III) in oxic seawater and to the fact that a large fraction of the limited iron available is already tightly complexed (Bruland *et al*., 1991). Indeed, iron availability is now well known to limit primary productivity in certain oceanic regimes (Martin and Fitzwater, 1988). While there is some evidence that marine algae produce siderophore-like molecules (Trick *et al*., 1983; Naito *et al*., 2001), to date not a single extracellular metal chelator produced by eukaryotic algae has been characterized, and ambiguity remains about whether the siderophore-like molecules purported to be isolated from cultures of eukaryotic algae are actually produced by the algae themselves or by associated bacteria.

While efficient transport mechanisms for iron uptake are an essential element in all pro- and eukaryotic cells, its intracellular availability and storage have to be tightly regulated, not only to buffer supply and demand, but also to prevent cell damage from undesirable reactions of free radicals, formed catalytically by free Fe ions. Ferritin represents the most common form of iron storage in all domains of life. This water-soluble protein is composed of a tetraeicosameric shell built up of polypeptide subunits and a microcrystalline core of ferrihydrite within the protein cavity. A general structural model of ferritins has been derived from X-ray diffraction studies (Ford *et al*., 1984; Harrison *et al*., 1989; Lawson *et al*., 1991; Frolow *et al*., 1994; Trikha *et al*., 1994). Although the general topology of most ferritins is similar, a remarkable heterogeneity of the ferritin subunits is observed which is the basis of different classes of ferritins including various types of bacterial ferritins, namely haem-containing bacterioferritins (Bfrs), non-haem bacterial ferritins Ftn1 and Ftn2, 'miniferritins' (exhibiting a dodecahedral peptide assembly), and various animal and plant 'maxiferritins'. Numerous functions have been attributed to these ferritins. One function is associated with 'true' iron storage. Under iron-rich growth conditions the metal is accumulated in order to provide an iron pool sufficiently high to prevent growth limitation effects in an iron-deficient environment. A second function is associated with the potentially harmful role iron can play in cell physiology by generating $OH^{\cdot -}$ and other oxygen radicals (Haber–Weiss–Fenton reaction cycle) (Matzanke, 1997). These oxygen radicals, and in particular $OH^{\cdot}$, may cause cellular oxidative damage and therefore participate in ageing processes and carcinogenesis (Halliwell and Gutteridge, 2007). A role for ferritin against oxidative stress has been shown in *Arabidopsis* (Ravet *et al*., 2009).

Brown algae (Phaeophyta) belong to a lineage that has been evolving independently of other major photosynthetic lineages, such as green plants (Chlorophyta) and red algae (Rhodophyta). Instead, they are classified within the Stramenopiles and Chromalveolates together with diatoms, golden-brown algae, and oomycetes (Baldauf, 2003). As a consequence of this singular evolutionary history, brown algae exhibit many unusual, and often unique, features. These features are adaptations to the marine coastal environments in which brown algae are usually the dominant organisms in terms of biomass, often forming extensive kelp forests. The key role of kelp forests, effectively constituting an interface between the ocean, the atmosphere, and land masses, in the biogeochemical cycle of halogens is well established (Küpper *et al*., 2008). However, the role of trace metals in brown algal-dominated ecosystems is poorly understood (as is brown algal trace metal metabolism), contrasting with the intense research interest which pelagic systems have received. This lack of knowledge is surprising in view of the fact that the industrial exploitation of brown algae is expanding partially due to interest in their use for production of alginate, fucans etc., but increasingly for their potential as biofuel where they have the advantage of high productivity without competing with terrestrial crops for farmland.

Ectocarpus siliculosus is a filamentous brown alga with a worldwide distribution along temperate coastlines, and is a nuisance as a 'fouling' organism on many man-made surfaces in the sea. It has some significant advantages as an experimental model and constitutes one of the best-studied seaweeds (Peters *et al*., 2004; Charrier *et al*., 2008). It can easily be cultivated in small volumes of seawater media both axenically and with associated bacteria, its entire, well-known life cycle can be completed within a few months in culture (Müller *et al*., 2008), and many molecular tools are available, including mutant collections, microarrays, and proteomics data. It has also recently become the first seaweed of which the entire genome has been sequenced and thus offers unprecedented opportunities for study (Cock *et al*., 2010).

While modern spectroscopic techniques such as Mössbauer spectroscopy and X-ray absorption spectroscopy (XAS) have played a major role in our understanding of iron uptake and storage in many terrestrial microorganisms (Winkler *et al*., 1994; Schünemann and Winkler, 2000; Matzanke *et al*., 2011), they have been little utilized in marine algal systems. Such spectroscopic techniques are powerful, non-invasive tools for the determination of both the *in vivo* redox, spin state, and coordination environment of iron, as well as for isolated biological (macro) molecules. Transmission Mössbauer spectroscopy (TMS) is valuable as it is specific for ^{57}Fe and thus no other transition metal obscures the experimental results. Due to the low natural abundance of the isotope (2%), ^{57}Fe enrichment is essential for almost any biological sample. This potential disadvantage, however, can be successfully exploited for iron uptake analyses since a sample prior to uptake typically exhibits ^{57}Fe in quantities below the detection limit of conventional Mössbauer spectroscopy. Thus only labelled newly acquired Fe is visible. XAS confirms and broadens the information obtained by Mössbauer. From XANES (X-ray absorption near edge structure), the average oxidation state of the metal centre and the metal ligand coordination geometry can be derived. Extended X-ray absorption fine structure (EXAFS) analysis provides metal–ligand bond distances at a high accuracy (±0.02 Å), metal–ligand type, and coordination number of the complex (albeit with lower accuracy, i.e. error bars of at least ±0.5). Herein the first ever study of the iron uptake and storage mechanisms in the brown alga *E. siliculosus* using such spectroscopic techniques in concert with more conventional radiolabelled uptake studies is reported.

Materials and methods

Ectocarpus siliculosus strain EcSil NZ KU 1–3♂ (CCAP 1310NZ1310-56) was obtained from the Culture Collection of Algae and Protozoa (CCAP) at the Scottish Association for Marine Science

and grown axenically in modified Provasoli-enriched (Andersen, 2005) Scripps Pier seawater (SPSW) at 17 °C with a 12 h:12 h light:dark photocycle. The iron content of SPSW was determined to be ~4 nM and is thus defined as the concentration for iron-limited growth. Prior to all experiments, *Ectocarpus* was starved for a period of 5–10 d under iron-limited conditions. Iron-replete conditions were obtained by adding Fe-EDTA to SPSW at 30 μM.

Cell surface reductase activity

Cell surface reductase activity was determined as described by Kranzler *et al*. (2011) using C18 Sep-Pak columns (Waters) which absorb the $^{55}Fe(FZ)_3$ complex formed by reduction of ^{55}FeEDTA in the presence of an excess of the Fe(II)-specific chelator ferrozine (FZ). After elution from the column with methanol, the $^{55}Fe(FZ)_3$ was quantified by liquid scintillation counting as described below.

Iron uptake studies

$^{55}FeCl_3$ radionuclide was obtained from Perkin-Elmer and used to prepare the ^{55}FeEDTA solution used as an iron source. To remove any surface-adsorbed Fe(III) species, *Ectocarpus* samples were strained, and washed with 50 ml of artificial seawater (ASW), followed by 10 ml of a titanium (III) citrate/EDTA solution prepared as described by Hudson and Morel (1989). This was followed by a final wash with 50 ml of ASW to remove all traces of Fe(II). Samples were then filtered onto 10 μm Millipore™ polycarbonate filters and washed with 50 ml of ASW under a vacuum. Thorough washing with both the titanium (Ti) reagent and subsequently with ASW is essential to eliminate artefacts caused by surface binding. Filters containing *Ectocarpus* were placed in scintillation vials and 1 ml of sodium hypochlorite was added to bleach the chlorophyll and reduce quenching effects. Vials were then heated in a 55 °C water bath for 1 h and left to vent overnight at room temperature to allow chlorine evaporation. A 15 ml aliquot of Hionic Fluor liquid scintillation fluid (Perkin-Elmer) was added to each of the vials which were incubated in the dark for at least 2 h to eliminate any background chemiluminesence. The ^{55}Fe taken up was measured on a Beckman-Coulter LS 6500 scintillation counter using the tritium channel. Total iron uptake per mg wet weight *Ectocarpus* was calculated based on specific activity, measured count rates, scintillation counting efficiency, and biomass measurements. For inhibition studies, azide, carbonyl cyanide 3-chlorohydrazine (CCCP), ascorbate, FZ, and the ionophores gramicidin and valinomycin were added to separate iron-limited cultures 1 h prior to inoculation with ^{55}FeEDTA.

Histochemistry

Ectocarpus siliculosus was grown under iron-replete conditions prior to fixation, dehydration, and embedding. Cells were fixated in a 0.1 M phosphate buffer solution containing 2% (w/v) paraformaldehyde, 1% (w/v) glutaraldehyde, and 1% (w/v) caffeine for 2 h. The fixed cells were then washed with 0.1 M phosphate buffer and dehydrated in successive ethanol baths of 30, 50, 75, 85, 95, and 100% (three times). The cells were then embedded in 1:1 (v/v) ethanol/LR White resin (LWR; EMS, Hatfield, PA, USA) for 3 h followed by 100% LWR overnight in gelatin capsules under vacuum. Sections of 3 μm were cut on a Leica EMUC6 microtome and deposited on glass slides. The Perls staining and diaminobenzidine (DAB) intensification procedure was performed as described by Meguro *et al*. (2007) and Roschzttardtz *et al*. (2009, 2010). Briefly, sections were incubated on glass slides with equal volumes of 4% (v/v) HCl and 4% potassium ferrocyanide (Perls staining solution) for 45 min. After washing with distilled H_2O, sections were incubated in a methanol solution containing 0.01 M NaN_3 and 0.3% (v/v) H_2O_2 for 1 h and then washed with 0.1 M phosphate buffer. DAB intensification was achieved by incubating sections in a 0.1 M phosphate buffer solution containing 0.00025–0.005% (w/v) DAB (Sigma), 0.005% (v/v) H_2O_2, and 0.005% (w/v) $CoCl_2$ for 30 min. The sections were then washed with H_2O before imaging with a Zeiss Axiovert 40 inverted microscope.

Transmission Mössbauer spectroscopy (TMS)

For TMS, *Ectocarpus* was grown for 33 d in modified Provasoli-enriched seawater containing 30 μM ^{57}FeEDTA. ^{57}Fe was obtained as the oxide from Isoflex (San Francisco, CA, USA) and converted to the chloride by repeated dissolution in concentrated HCl. The chloride was subsequently added to a concentrated solution of EDTA and the pH adjusted to 6.0. Algal samples were washed with the Ti citrate/EDTA reagent in order to remove adventitious iron from the algal surface, and the cells were harvested by vacuum-assisted filtration. Pellets were weighed, transferred into Delrin® Mössbauer sample holders, frozen in liquid nitrogen, and kept at this temperature until measurement, except for overnight transport on dry ice. The Mössbauer spectra were recorded in the horizontal transmission geometry using a constant acceleration spectrometer operated in conjunction with a 512-channel analyser in the time-scale mode. The detector consisted of a proportional counter filled with argon–methane (9:1). The source was at room temperature and consisted of 1.4 GBq (^{57}Co) diffused in Rh foil (WissEl, Starnberg, Germany). The spectrometer was calibrated against α-iron at room temperature. For measurements at 77K, samples were placed in a continuous-flow cryostat (Oxford Instruments). For measurements at 4.3K and 2K, a helium bath cryostat (MD306, Oxford Instruments) was employed. Spectral data were transferred from the multichannel analyser to a PC for further analysis employing the public domain Vinda program on an Excel 2003® platform. Isomer shift δ, quadrupole splitting ΔE_Q, B_{hf}, and percentage of the total absorption area were obtained by least-squares fits of Lorentzian lines to the experimental spectra. All values are rounded to the last given digit. The isomer shifts (δ), the quadrupole splitting (ΔE_Q), and the line width (Γ) are given in mm s^{-1}. The relative area is given in parts per hundreds.

EXAFS

Spectra were measured at Doris III, beamline A1 (DESY, Hamburg, Germany) using a fluorescence detector. Frozen samples were measured in a continuous flow cryostat (Oxford Instruments, Optistat) at 12K. The energy was calibrated in transmission mode against an iron foil while experimental spectra were recorded in the fluorescence mode. Algal samples were prepared as described above, and samples CC45 (Mössbauer) and CC47 (EXAFS) were prepared from the same batch. During sample handling, the sample temperature was kept below 195K.Thirty-nine energy scans from 6960 eV to 8112 eV were performed, resulting in 52 spectra. Spectra obtained during ring filling were skipped. Each scan was performed as follows: from 6960 eV to 7085 eV the energy step E was 5 eV, from 7085 eV to 7152 eV ΔE was 0.5 eV, and from 7152 eV to 8112 eV non-equidistant energy steps were used starting at ΔE=0.8 eV. In the first two regions, a sampling time of 1 s was used. In the third region, an increasing sampling time was used corresponding to the non-equidistant energy steps starting at 1 s.

In each spectrum, the K-edge was localized by the zero crossing of the second derivative of the fluorescence signal and corrected against the iron foil K-edge. All spectra were summed up prior to correction. Afterwards, the sum was corrected as follows: the pre-edge range was defined relative to the determined K-edge from –150 eV to –30 eV and fitted with a line. The post-edge range for normalization was set relative to the K-edge from +150 eV to +880 eV and was fitted with a quadratic polynomial. The sum spectrum was corrected for its background, its pre-edge, and normalized to its post-edge. Forward Fourier transformation was performed for a k-range from 2 $Å^{-1}$ to 8.5 $Å^{-1}$ using a Hanning window function. The final overall fit of the two-component model (see below) uses scattering paths with distances <3.4 Å. The fits were performed in R-space using a Hanning type window from r=1.2 Å to 3.35 Å. For the least square fits in R-space, a k-weight of 2 was used. All corrections and fits were performed by the Athena/Artmis program package of Ravel (2005).

Results

Cell surface reductase activity

With the detection of a putative cell surface reductase in the *Ectocarpus* genome (Cock *et al*., 2010), experimental confirmation

of external Fe(III) chelate reduction was sought. For these experiments, *Ectocarpus* cells previously grown under either iron-replete (30 μM) or limited (4 nM) conditions (see the Materials and methods) were incubated in the presence of 30 μM ^{55}Fe FeEDTA and 100 μM of the Fe(II)-specific chelator FZ for 24 h. Cells were then harvested and the $^{55}Fe(FZ)_3$ complex formed in the supernatant assayed as described by Kranzler *et al*. (2011). As can be seen from Fig. 1, live, iron-limited, *Ectocarpus* cells were readily capable of reducing Fe(III) in the form of an EDTA complex at a rate of ~1 ng Fe mg^{-1} h^{-1}, that is commensurate with that of overall iron uptake (see below). Dead cells exhibited no activity, indicating that iron reduction was a specific metabolic process rather than a non-specific process driven by the presence of FZ. Under iron-replete conditions, ferric chelate reduction was reduced by almost half, suggesting that the reductase activity is inducible.

Iron uptake

Iron 'uptake' without the Ti washing procedure described in the Materials and methods was always very high and time independent; observations that are consistent with strong, non-specific, cell surface binding. This non-specific binding was confirmed by TMS which showed a very strong signal with spectral parameters distinct from those much weaker signals seen following the Ti wash (see below). Careful and extensive washing of the cells with ASW following the Ti wash was also required to prevent the artefactual observation of residual surface-bound Fe(II) by TMS. However, with the appropriate care, ^{55}Fe from FeEDTA was seen to be taken up by iron-starved *Ectocarpus* in a time-dependent fashion. Uptake was relatively rapid (0.44 ng mg^{-1} h^{-1}) and approximately linear for ~24 h, after which the uptake rate slowed and eventually ceased (Fig. 2). The uptake process appeared to be an active one as it was inhibited by a number of metabolic poisons or environmental effects. Pre-treatment of cells with azide, CCCP, ascorbate, gramicidin, or valinomycin resulted in 25–90% uptake inhibition (data not shown), whereas FZ had no effect. The uptake process was also saturable as

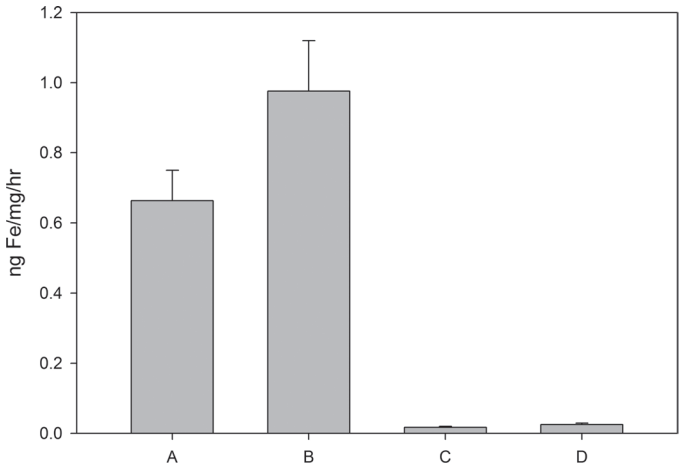

Fig. 1. Fe(III) chelate reductase activity for (A) iron-replete (30 μM) and (B) iron-starved (4 nM) cultures of *Ectocarpus siliculosus* grown as described in the Materials and methods. (C) Dead cells and (D) live cells minus FZ represent negative controls. Error bars represent ±1 SD from triplicate measurements.

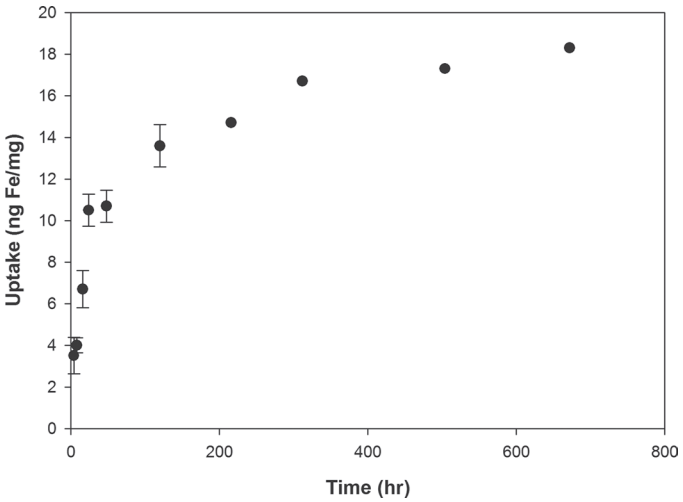

Fig. 2. Iron uptake from ^{55}FeEDTA as a function of time in *Ectocarpus siliculosus* cultures over 800 h. Error bars represent ±1 SD from three separate experiments with replicate time points for each.

determined by its concentration dependence (Fig. 3) the data of which could be fit well (R^2=0.9939) to a model with a V_{max} of 1.47 ± 0.15 ng mg^{-1} h^{-1}, and a K_m of 1.5 ± 0.5 μM.

FeEDTA was used as an iron source as it is generally thought that the intact FeEDTA complex is not a biological substrate but rather it serves as an iron buffer maintaining a fixed concentration of free soluble Fe(III) known as Fe(III)' at equilibrium while preventing the precipitation of insoluble Fe oxo-hydroxo polymeric species. To test the suitability of this hypothesis with *Ectocarpus*, the iron uptake rate at a fixed concentration of iron as a function of an increasing EDTA to Fe ratio was determined. Increasing the EDTA to Fe ratio should increase the concentration of FeEDTA and decrease the concentration of free Fe(III) at equilibrium. Thus, if FeEDTA itself was the biological substrate, the uptake rate should increase, while if free Fe(III) was the substrate, then uptake should decrease. Upon going from an EDTA/Fe ratio of 1.5:1 to 100:1, a 50-fold decrease in the uptake rate was observed, consistent with the idea that FeEDTA is serving simply as an iron buffer and the species actively involved in uptake is free Fe(III)'.

Histochemistry

Using the Perls–DAB staining protocol described by Roschzttardtz *et al*. (2009, 2010), it is possible to visualize the localization of iron at the subcellular level. The highest levels of iron consistently appeared as small dark granules clustered together inside the cell and not associated with the plastids, which in *Ectocarpus* typically adopt a spiral banded pattern (Fig. 4). Control cell slices not treated with Perls–DAB do not show such a staining pattern. While the exact nature of the structures that contain the majority of iron remains obscure, it is clear that large concentrations of iron appear to be stored inside *Ectocarpus* cells.

Mössbauer spectroscopy

After long-term incubation with ^{57}FeEDTA, TMS spectra exhibiting sufficient resonance absorption were obtained which display

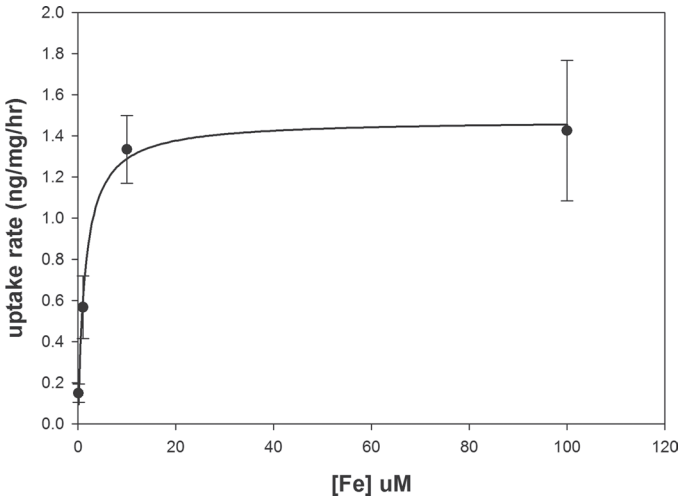

Fig. 3. Concentration-dependent uptake of iron from ^{55}FeEDTA after 24 h by *Ectocarpus siliculosus.* Error bars represent ±1 SD from duplicate experiments with replicate concentration points for each.

a single quadrupole doublet-like feature (Fig. 5). Since the algal filament was thoroughly washed with the Ti citrate/EDTA reagent, the presence of iron on the algal surfaces can be excluded and, therefore, the iron components observed by TMS are genuinely of intracellular origin. From this, it can be concluded that ^{57}Fe supplied as the EDTA complex in the medium is transported into, and metabolized inside, cells of *Ectocarpus*. However, despite its seeming simplicity, detailed analysis of the TMS spectrum showed the presence of two different and distinct iron species. The first corresponds to an $(Fe_4S_4)^{2+}$ cluster. Biological $[Fe_4S_4]^{n+}$ clusters are typically found in three cluster oxidation states: 1+, 2+, and 3+ (Schünemann and Winkler, 2000). All three types of $[Fe_4S_4]$ cluster exhibit characteristic Mössbauer parameters which can be distinguished in most cases quite well. An iron–sulphur cluster in the +2 state displays at 4.3K isomer shifts in the range from 0.39 mm s^{-1} to 0.45 mm s^{-1} and quadrupole splittings from 0.98 mm s^{-1} to 1.22 mm s^{-1}. Isomer shift and quadrupole splitting of the iron–sulphur species in the *in situ* Mössbauer spectrum of *E. siliculosus* are in the range found for such a cluster (26% of the absorption area, Table 1). This iron–sulphur cluster very probably represents a component of chloroplast and/or mitochondrial redox systems. The second iron compound detected by TMS displays a spectrum typical of a polymeric $(Fe^{3+}O_6)$ system which accounts for 74% of the absorption area (Table 1, Fig. 5). Polymeric biological $(Fe^{3+}O_6)$ systems found by *in situ* Mössbauer spectra very often represent the mineral cores of ferritins. The Mössbauer spectroscopic features of such systems are strongly temperature and size dependent, reflecting superparamagnetic relaxation of magnetic nanoparticles (Mørup, 2011). Bacterial ferritins (Bfr and Ftn) typically show superparamagnetic splitting (doublet–sextet transition) at temperatures below 4.3K, indicating an amorphous and frequently phosphate-rich crystal structure (Bauminger *et al*., 1980*a*, *b*; Mann *et al*., 1987; Matzanke, 1997; Reindel *et al*., 2002; Boughamoura *et al*., 2008). The sextet lines show one-third of the resonance absorption compared with the doublet lines, and are, in addition, considerably broadened due to particle size distributions of the mineral. The Mössbauer

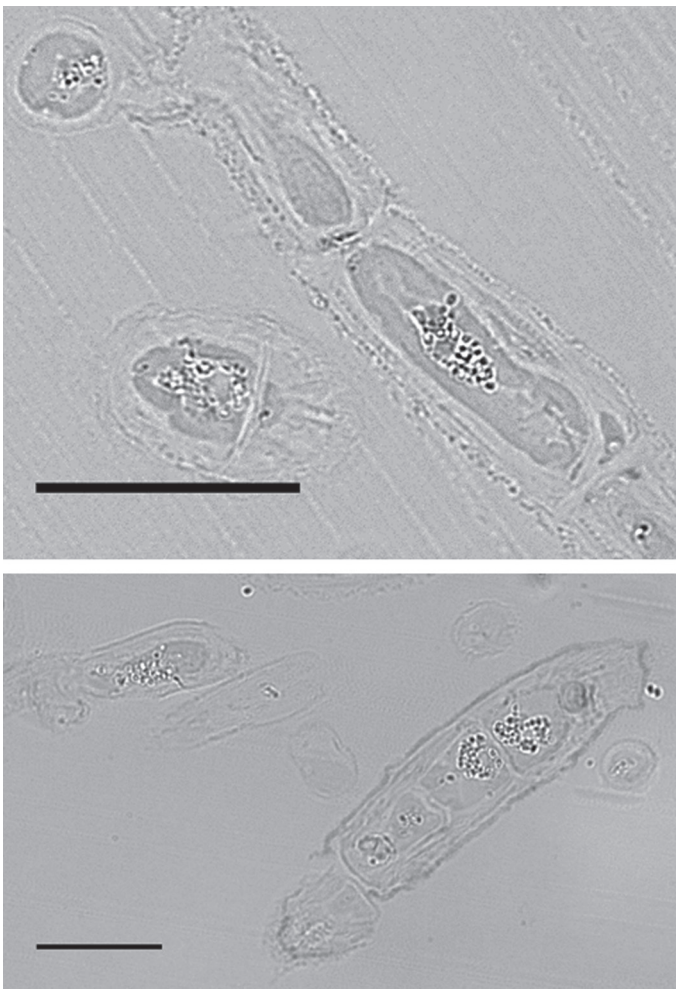

Fig. 4. Micrographs (×63) of 3 µm sections of *Ectocarpus* cells embedded in LWR and stained by the Perls–DAB procedure as outlined in the Materials and methods. Upper panel: treatment at pH 7 with 0.0025% DAB. Lower panel: treatment at pH 1 with 0.005% DAB. The scale bars are 20 µm and the dark grains represent high concentrations of iron. (This figure is available in colour at *JXB* online.)

spectrum of *Ectocarpus* at 1.8K shows less resonance absorption in the centre part compared with that seen at 4.3K (0.2 transmission intensity as compared with 0.45), indicating the partial disappearance of one doublet. The disappearance of the $(Fe^{3+}O_6)$ doublet can only be explained (since the Lamb–Mössbauer factor, f, at 1.8K cannot be smaller than that at 4.3K) by the formation of a broadened six-line pattern; the result of a doublet–sextet transition as found in bacterial ferritins. However, due to the low intensity of the $(Fe^{3+}O_6)$ doublet lines, the six-line pattern is at the detection limits of TMS (0.1% effect per line or even less). The residual absorption at 1.8K could be adequately fit with just the iron–sulphur species.

XAS

In addition to TMS, XAS was employed to probe the chemical nature of the internalized iron. Based on the above Mössbauer

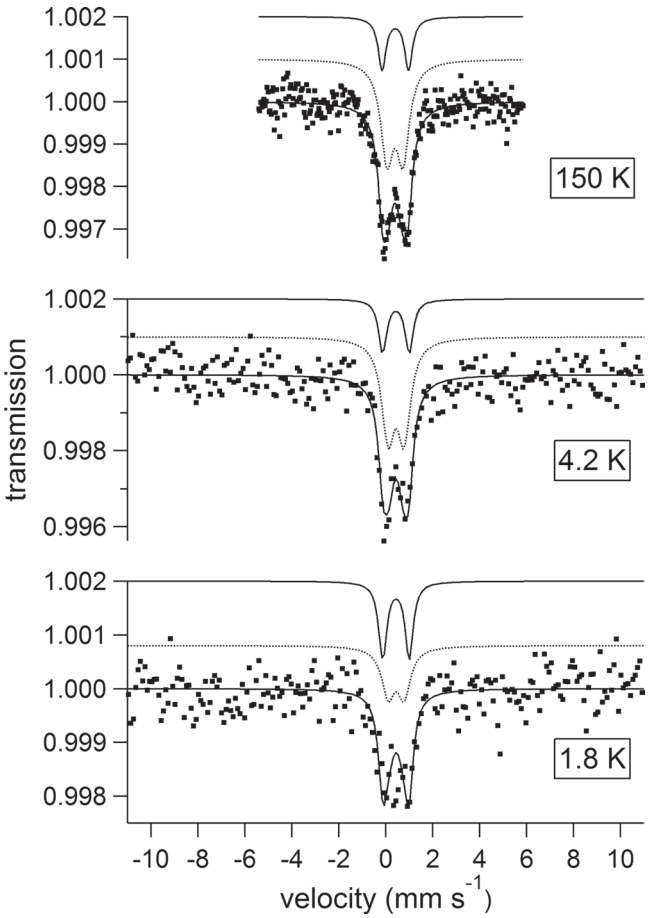

Fig. 5. Mössbauer spectra of *Ectocarpus siliculosus* at 150K (upper), 4.3K (middle), and 1.8K (lower). The filled squares represent the experimental data. The subspectra obtained by least squares fits of Lorentzian lines are depicted by the light grey solid line (Fe_4S_4) and dark grey dotted line (polymeric FeO_6). The black solid line represents the overall fit. (This figure is available in colour at *JXB* online.)

data, the presence of a superparamagnetically coupled polymeric Fe^{3+}-oxo system and of an $[Fe_4S_4]^{2+}$ cluster was indicated. Within this constraint, various models were tested. For the Fe^{3+}-oxo species, the models tested included ferric (oxo, oxo-organic, oxo-phosphate), ferrihydrite, ferric phosphate, and FeO(OH). Models for these species were constructed and coordinates obtained after molecular mechanics energy minimization using the program Chem 3D. These coordinates were then used as input in the FEFF program to obtain the scattering paths. The best fits came from the oxo-phosphate model. However, the resulting fits were still unsatisfactory when only oxo-phosphate ligands were employed in the first ligand sphere. There was definitely an iron–sulphur contribution which was consistent with the Mössbauer spectra. Structural data for various iron–sulphur clusters were extracted from the appropriate data banks, and coordinates extracted after molecular mechanics energy minimization using the Program Chem3D. The resulting coordinates were again used for input in the FEFF program to obtain the scattering paths. Acceptable fits were only obtained for an $[Fe_4S_4]^{2+}$ cluster.

The final fit of the EXAFS spectrum (Figs 6, 7) to the two-component model {i.e. polymeric Fe(III) oxo-phosphate and an $[Fe_4S_4]^{2+}$ cluster} was very good where the second coordination shell of the Fe-oxo species contains 3.5 ± 0.5 P and 1 ± 0.5 Fe (Table 2). The Fe-oxo species comprises ~74% and the Fe–S species ~26% of the total iron. The average bond distances obtained from the EXAFS fit are summarized in Table 2. Attempts to add additional components such as an $[Fe_2S_2]^{2+}$ (or additional Fe-oxo species) provided no statistically significant improvement to the fit. Overall, the EXAFS fit data are completely consistent with those obtained by TMS. In particular, they support both quantitatively and qualitatively the polymeric nature of the iron oxo species and the presence of an iron–sulphur protein as suggested by the Mössbauer spectra.

Discussion

Uptake

In bacteria there are a myriad of uptake systems and acquisition strategies designed to capture iron, many of which are often simultaneously operative in a single organism. These include uptake systems specific for siderophores, or other bound forms of iron (a similar system is also found in strategy II plants) as well as those based on ABC-type transporters capable of taking up 'free' Fe(III) and other transporters typically more or less specific for ferrous iron (Dassa and Bouige, 2001; Koester, 2001). Model eukaryotes typically adopt iron uptake schemes which involve reduction of Fe(III) to Fe(II) at some point, although there appear to be exceptions (Sutak *et al*., 2010). The first of these mechanisms is a reductive–oxidative pathway such as that found in yeast (Curie and Briat, 2003) and some green algae (La Fontaine *et al*., 2002), and the second is a cell surface reduction/divalent metal permease pathway such as that found in strategy I plants (Bauer and Bereczky, 2003; Morrissey and Guerinot, 2009; Weger *et al*., 2009; Sonier and Weger, 2010). Among the marine algae, the iron uptake systems of the diatoms have been the most thoroughly studied (Shaked *et al*., 2005; Kustka *et al*., 2007). Iron uptake in these related organisms has been described by the so-called Fe(II)s mechanism (Shaked *et al*., 2005) where reduction of free Fe(III)' is the seminal step. This reductive step is followed either by direct uptake of the formed Fe(II) as in the pennate diatom *Phaeodactylum tricornutum* or by reoxidation of the Fe(II) by a multicopper oxidase and transport as Fe(III) as in the centric diatom *Thalassiosira pseudonana* (Kustka *et al*., 2007).

Genomic data suggest that *Ectocarpus* may, with some variation, use one or more of these approaches. In particular, Cock *et al*. (2010) have identified homologues of *fro2*, a proposed cell surface Fe(III) reductase. This Fe(III) reductase activity was also experimentally verified and its rate was commensurate with that of the overall iron uptake process. Additionally homologues to several divalent metal ABC transporters could be found (Bauer and Bereczky, 2003; Curie and Briat, 2003; Morrissey and Guerinot, 2009) as well as NRAMP, an M^{2+}–H^+ symporter with a preference for Fe(II) (Bauer and Bereczky, 2003; Curie and Briat, 2003; Morrissey and Guerinot, 2009), which would be consistent with the simple reductase/permease pathway. While

Table 1. Mössbauer fit parameters of isomer shift (δ), quadrupole splitting (ΔE_Q), linewidth (Γ), and percentage of absorption area of *E. siliculosus* (CC45) at 150, 4.2, and 1.8K

The error in the last digit is 0.04 mm s^{-1}.

	Parameter	In mm s^{-1} at 1.8K	In mm s^{-1} at 4.2K	In mm s^{-1} at 150K
$[Fe^{3+}O_6X_m^n]^{mn-9}$	δ	0.44	0.44	0.39
	ΔE_Q	0.68	0.68	0.68
	Γ	0.66	0.66	0.66
	Area	50%	74%	74%
$[Fe_4\text{-}S_4]^{2+}$	δ	0.43	0.43	0.40
	ΔE_Q	1.13	1.13	1.13
	Γ	0.41	0.41	0.41
	Area	50%	26%	26%
SQRT		0.86	0.79	0.80

Table 2. Average distances and numbers of first and second shell ligands in Fe–O and Fe–S iron centres of sample CC47 obtained from the EXAFS fit as described in the text

The accuracy for ligand numbers *n* is ±0.5.

	Fe–O	Fe–(O)–P	Fe–(O)–Fe	Fe–S	Fe–(S)–Fe
Å	1.96	3.07	3.35	2.11	2.64
n	6	3.5	1	4	3

Elements in parentheses display bond angles indicating that the Fe–(X)–Y distance is shorter than the summation of individual bond lengths.

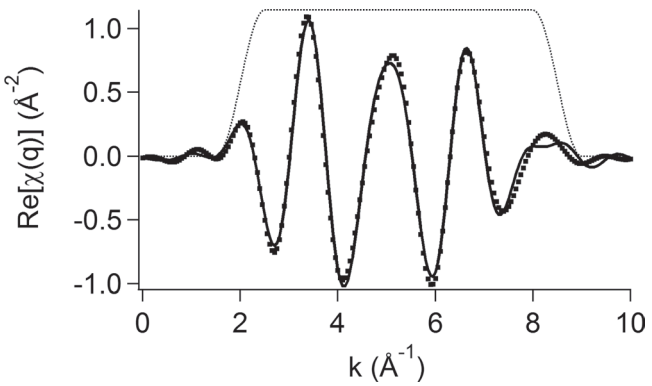

Fig. 6. Extracted EXAFS spectrum of 52 merged spectra transformed in q-space. The filled squares represent experimental data, the black solid line represents the fit, and the light grey dotted line depicts the setting of the range. (This figure is available in colour at *JXB* online.)

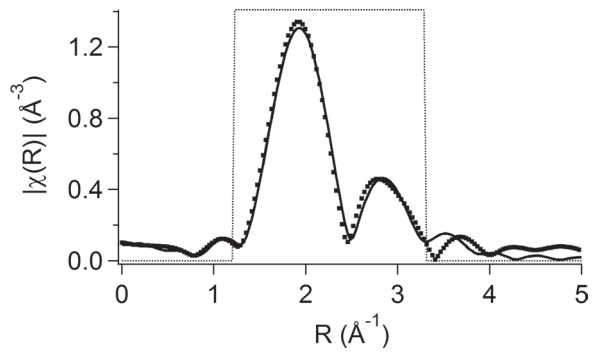

Fig. 7. EXAFS data of CC47 plotted in R-space. The graph was plotted with a k-weight of 1 and a phase correction. The k-range for the fast Fourier transformation was 2 $Å^{-1}$ to 8.5 $Å^{-1}$. The fit was performed with a model containing FeO_6 and Fe_4S_4 structures due to the limited R range up to *r*=3.35 Å as described in the text. Filled squares represent experimental data, the black solid line the fit, and the light grey dotted line the setting of the range.

no direct homologues to the multicopper oxidases (MCOs) Fox1 from *Chlamydomonas* or Fet3 of *T. pseudonana* could be found, two genes annotated as MCOs implicated in iron transport can be found in the *Ectocarpus* genome.

Short-term iron uptake studies verified that iron is taken up by *Ectocarpus* in a time-and concentration-dependent manner consistent with an active transport process. Derived kinetic parameters (Table 3) are qualitatively and quantitatively similar to those reported in the few available studies of other red, green, and brown algae (Manley, 1981; Matsunaga *et al*., 1991; Liu *et al*., 2000). While it is difficult to compare V_{max} rates due to the differing units employed in each of these studies as well as the different surface/volume ratios of the model organisms, the uptake rate for the slow growing *Ectocarpus* is similar that seen in *Gracilaria* and approximately an order of magnitude less than that of the faster growing *Chlamydomonas*, *Laminaria*, and *Macrocystis* (Manley, 1981; Matsunaga *et al*., 1991; Liu *et al*., 2000). However, the affinity constant (K_m) of ~1.5 μM is similar to the others which range from 0.1 to 3 μM. While open ocean iron concentrations are typically subnanomolar (Johnson *et al*., 1997), near-shore coastal areas can have iron concentrations orders of magnitude higher; that is, hundreds of nanomolar (Chase *et al*., 2002). Thus the affinity constants (based on total iron) seen for near-shore-dwelling macroalgae in the lower micromolar to high nanomolar range would appear to be reasonable. However, it should be noted that if free soluble Fe(III)' rather than Fe(EDTA) itself is the actual substrate, as indicated by the constant Fe-variable EDTA concentration data presented

Table 3. Transport parameters for iron uptake in marine algae

	Macrocystis	*Gracilaria*	*Laminaria*	*Undaria*	*Ectocarpus*
V_{max}	1.6 pmol cm^{-2} h^{-1}	0.26 pmol mg^{-1} h^{-1}	2.7 pmol cm^{-2} h^{-1}	6.4 pmol cm^{-2} h^{-1}	0.25 pmol mg^{-1} h^{-1}
K_m	3.5 μM	0.6 μM	0.54 μM	6.4 μM	1.5 μM
Reference	Manley (1981)	Liu *et al*. (2000)	Matsunaga *et al*. (1991)	Matsunaga *et al*. (1991)	This work

earlier, then the true affinity constant is probably subnanomolar. However, the data are reported on the basis of total iron concentration in order to facilitate comparison with previous work (Manley, 1981; Matsunaga *et al*., 1991; Liu *et al*., 2000).

Although an initial reductive process is clearly indicated both genomically and experimentally, whether the iron is taken up directly as Fe(II) or reoxidized and transported as Fe(III) (see above) remains unclear. While the lack of inhibition of iron uptake by FZ is surprising assuming a reductive process being operative, at the concentrations tested (50 μM) there is insufficient FZ to sequester completely all the Fe(II) formed via the reductase as a $Fe(FZ)_3$ complex. Since the rate of reduction appears to exceed that of actual uptake, there would remain a sufficient pool of uncomplexed Fe(II) to support continued uptake. It is also possible that the Fe(II) produced by the reductase is tightly coupled with an oxidase (see below) so that the ferrous ion is never in free equilibrium with the bulk solution and thus is unaffected by the presence of an external Fe(II) chelator. The strong inhibition by ascorbate, which at first glance also seems counter-intuitive, suggests that a reductive/oxidative pathway may be the operative one as the ascorbate could be expected to inactivate a multicopper oxidase.

Unfortunately, attempts to determine the oxidation state of the initially transported iron by TMS were thwarted by the low sensitivity of the technique. Thus incubation times of the order of weeks in ^{57}Fe-enriched solutions are required to obtain useable spectra. This precluded following short-term iron uptake processes by this method. It was possible, however, to use TMS and XAS to provide evidence as to the fate of the transported iron after longer term exposure (3–4 weeks).

Storage

The first and most obvious conclusion from the long-term incubation studies is the lack of an observable ferrous iron pool in *Ectocarpus*. In previous *in vivo* Mössbauer studies of various bacterial, fungal, plant, and algal systems, significant amounts of intracellular high-spin ferrous iron octahedrally coordinated by oxygen ligands could be detected (Boenke and Matzanke, 1995; Semin *et al*., 2003; Matzanke *et al*., 2004, 2011; Kovacs *et al*., 2005, 2009). There is no evidence for such a species in *Ectocarpus*. Thus, despite the fact that the iron is probably transported across the cell membrane as Fe(II), it must be relatively rapidly reoxidized to Fe(III) and stored in that form. Of the two major metabolites which could be identified, one was an iron–sulphur protein which is likely to be a component of chloroplast and/or mitochondrial redox systems. However, a storage role for this species cannot be eliminated since in some archaeal systems polyferredoxins were detected, whose physiological function, while unclear, has been hypothesized to be to serve as electron sinks (Nölling et al., 1995; Wasserfallen *et al*., 1995). Nevertheless, the vast majority of organisms store iron in one or more of the various forms of the ubiquitous protein ferritin. However, genomic analysis reveals the presence of no ferritin or ferritin-like homologues in *Ectocarpus* (Cock *et al*., 2010). While this is unusual, it is not unprecedented. Thus while some diatoms such as *P. tricornutum* have ferritin genes, they have not been detected in others such as *T. pseudonana* (Marchetti *et al*., 2009).

In the absence of ferritins, two alternative or additional forms of iron storage have been identified in other organisms. The first, found in some fungi, is a siderophore-based storage system (Matzanke *et al*., 1987, 1988) clearly not present here. The second, which has been elucidated in yeast and several other eukaryotes including the halotolerant alga *Dunaliella salina*, is a vacuole based one (Martinoia *et al*., 2007; Paz *et al*., 2007). At present, there are few data in the literature about the chemical nature of vacuole sequestered iron stores. However, it seems likely that the iron would be stored in some sort of mineral phase. Indeed, it is reported that in *Arabidopsis* seeds some iron is located in vacuole globoids containing phytate which may bind ferric ions via phosphate groups (Lanquar *et al*., 2005) similar to what is proposed here. This notion is supported by the iron-specific histological staining which shows accumulation of high concentrations of granular-like iron stores inside *Ectocarpus* cells.

Since the spectroscopic parameters and relaxation properties (i.e. magnetic ordering temperatures) of condensed iron mineral phases are strongly dependent on particle sizes and their crystalline/amorphous structure, detailed temperature-dependent Mössbauer measurements can shed light on the nature of any iron stores. The observation that the second iron compound detected by TMS and XAS displays spectra typical of an ($Fe^{3+}O_6$) system with parameters similar to the amorphous, phosphorus-rich mineral core of bacterial and plant ferritins suggests that *Ectocarpus* does indeed contain a mineral phase iron storage form. Whether this mineral phase is in the form of a ferritin-like protein which lacks significant homology to previously studied systems, or is sequestered in some sort of vacuole, remains to be determined. Work geared towards more fully characterizing this system is in progress.

Acknowledgements

This work is supported by a joint USA–Germany International Chemistry Collaboration (ICC) grant: NSF CHE-0924313 to CJC and DFG Ma 916/20–1 to BFM. We acknowledge the support of the European Community research infrastructure action under the FP7 ‘capacities’ specific programme ASSEMBLE (grant no. 227788). We thank Professor Kathy Barbeau, SIO/UCSD and her students for determining the iron content of our Scripps Pier

water. LHB, CA, and BFM thank DESY, Hamburg for access to their infrastructure (DORIS III beamline at HASYLAB) making possible the EXAFS experiments. LHB thanks Dr E. Welter, HASYLAB, for scientific advice, and EPM and CJC thank Dr Steve Barlow, SDSU Microscopy Center, for help with the histochemistry and microscopy.

References

Andersen RA. 2005. *Algal culturing techniques*. Amsterdam: Elsevier Academic Press.

Baldauf SL. 2003. The deep roots of eukaryotes. *Science* **300,** 1703–1706.

Bauer P, Bereczky B. 2003. Gene networks involved in iron acquisition strategies in plants. *Agronomie* **23,** 447–454.

Bauminger ER, Cohen SG, Dickson DPE, Levy A, Ofer S, Yariv J. 1980*a*. Mössbauer spectroscopy of *Escherichia coli* and its iron storage protein. *Biochimica et Biophysica Acta* **623,** 237–242.

Bauminger ER, Cohen SG, Labenski de Kanter F, Levy A, Ofer S, Kessel M, Rottem A. 1980*b*. Iron storage in *Mycoplasma capriculum*. *Journal of Bacteriology* **141,** 378–381.

Böhnke R, Matzanke BF. 1995. The mobile ferrous iron pool in *E. coli* is bound to a phosphorylated sugar derivative. *BioMetals* **8,** 223–230.

Boughamoura A, Matzanke BF, Böttger L, Reverchon S, Lesuisse E, Expert D, Franza T. 2008. Differential role of ferritins in iron metabolism and virulence of the plant pathogenic bacterium *Erwinia chrysanthemii* 3937. *Journal of Bacteriology* **190,** 1518–1530.

Bruland KW, Donat JR, Hutchins DA. 1991. Interactive influences of bioactive trace metals on biological production in oceanic waters. *Limnology and Oceangraphy* **36,** 1555–1577.

Charrier B, Coelho SM, Le Bail A, Tonon T, Michel G, Potin P, Kloareg B, Boyen C, Peters AF, Cock JM. 2008. Development and physiology of the brown alga *Ectocarpus siliculosus*: two centuries of research. *New Phytologist* **177,** 319–332.

Chase Z, van Geen A, Kosro PM, Marra J, Wheeler PA. 2002. Iron nutrient and phytoplankton distributions in Oregon coastal waters. *Journal of Geophysical Research* **107,** 3174–3191.

Cock JM, Sterck L, Rouzé P, et al. 2010**.** The *Ectocarpus* genome and the independent evolution of multicellularity in the brown algae. *Nature* **465,** 617–621.

Curie C, Briat JF. 2003. Iron transport and signalling in plants. *Annual Reviews of Plant Biology* **54,** 183–206.

Dassa E, Bouige P. 2001. The ABC of ABCs: a phylogenetic and functional classification of the ABC systems in living organisms. *Research in Microbiology* **152,** 211–229.

Ford GC, Harrison PM, Rice JMA, Smith A, Treffry JL, White JL, Yariv J. 1984. Ferritin: design and formation of an iron-storage molecule. *Philosophical Transactions of the Royal Society B: Biological Sciences* **304,** 551–565.

Frolow F, Kalb AJ, Yariv J. 1994. Structure of a unique twofold symmetric haem-binding site. *Nature Structural Biology* **1,** 453–460.

Halliwell B, Gutteridge, JMC. 2007. *Free radicals in biology and medicine*. Oxford: Oxford University Press.

Harrison PM, Lilley TH. 1989. Ferritin. In: Loehr TM, ed. *Iron carriers and iron proteins*. New York: VCH Publishers, 123–238.

Hudson RJM, Morel FFM. 1989. Distinguishing between extra- and intracellular iron in marine phytoplankton. *Limnology and Oceangraphy* **34,** 1113–1120.

Johnson KS, Gordon RM, Coale KH. 1997. What controls dissolved iron concentrations in the world ocean? *Marine Chemistry* **57,** 137–161.

Köster W. 2001. ABC transporter-mediated uptake of iron, siderophores, heme, and vitamin B_{12}. *Research in Microbiology* **152,** 291–301.

Kovacs K, Kuzmann E, Fodor, F, Vertes A, Kamnev AA. 2005. Mössbauer study of iron uptake in cucumber root. *Hyperfine Interactions* **165,** 289–294.

Kovacs K, Kuzmann E, Tatar E, Vertes A, Fodor, F. 2009. Investigation of iron pools in cucumber roots by Mössbauer spectroscopy: direct evidence for strategy I iron uptake mechanism. *Planta* **229,** 271–278.

Kranzler C, Lis H, Shaked Y, Keren N. 2011. The role of reduction in iron uptake processes in a unicellular, planktonic cyanobacterium. *Environmental Microbiology* **13,** 2990–2999.

Küpper FC, Carpenter LJ, McFiggans GB, et al. 2008**.** Iodide accumulation provides kelp with an inorganic antioxidant impacting atmospheric chemistry. *Proceedings of the National Academy of Sciences, USA* **105,** 6954–6958.

Kustka AB, Allen AE, Morel FMM. 2007. Sequence analysis and transcriptional regulation of iron acquisition genes in two marine diatoms. *Journal of Phycology* **43,** 715–729.

La Fontaine S, Quinn JM, Nakamoto SS, Page MD, Göhre V, Moseley JL, Kropat J, Merchant S. 2002. Copper-dependent iron assimilation pathway in the model photosynthetic eukaryote *Chlamydomonas reinhardtii*. *Eukaryotic Cell* **1,** 736–757.

Lanquar V, Lelievre F, Bolte S, et al. 2005**.** Mobilization of vacuolar iron by AtNRAMP3 and AtNRAMP4 is essential for seed germination on low iron. *EMBO Journal* **24,** 4041–4051.

Lawson DM, Artymiuk PJ, Yewdall SJ, et al. 1991**.** Solving the structure of human H ferritin by genetically engineering intermolecular crystal contacts. *Nature* **349,** 541–544.

Liu, J, Dong S, Liu X, Ma S. 2000. Responses of the macroalga *Gracilaria tenuistipitata* var. liui (Rhodophyta) to iron stress. *Journal of Applied Phycology* **12,** 605–612.

Manley SL. 1981. Iron uptake and translocation by *Macrocycystis pyrifera*. *Plant Physiology* **68,** 914–918.

Mann S, Williams JM, Treffry A, Harrison P. 1987. Reconstituted and native iron cores of bacterioferritin and ferritin. *Journal of Molecular Biology* **198,** 405–416.

Marchetti A, Parker MS, Moccia LP, et al. 2009**.** Ferritin is used for iron storage in bloom forming marine pennate diatoms. *Nature* **457,** 467–470.

Martin JH, Fitzwater SE. 1988. Iron-deficiency limits phytoplankton growth in the Northeast Subarctic Pacific. *Nature* **331,** 341–343.

Martinoia E, Maeshima M, Neuhaus HE. 2007. Vacuolar transporters and their essential role in plant metabolism. *Journal of Experimental Botany* **58,** 83–102.

Matsunaga K, Suzuki Y, Kuma K, Kudo I. Nakabayshi S. 1991. Uptake rate of iron by macroalgae from the Sea of Japan. *Bulletin of the Japanese Society for Fisheries and Oceanography* **55,** 349–353.

Matzanke BF. 1997. Iron storage in microorganisms. In: Winkelmann G**,** Carrano C, eds. *Transition metals in microbial metabolism*. Harwood Academic Publishers, 117–157.

Matzanke BF, Anemüller S, Schünemann V, Trautwein AX, Hantke K. 2004. FhuF—the first example of a hydroxamate siderophore reductase. *Biochemistry* **43,** 1386–1392.

Matzanke BF, Brandenburger M, Böttger LH. 2011. Mössbauer spectroscopy of microbial iron metabolism. On DVD In: Gütlich P**,** Bill E, Trautwein AX, eds. *Mössbauer spectroscopy and transition metal chemistry*. Berlin: Springer-Verlag.

Matzanke BF, Bill E, Trautwein AX, Winkelmann G. 1988. Ferricrocin functions as the main intracellular iron-storage compound in mycelia of Neurospora crassa. *BioMetals* **1,** 18–25.

Matzanke BF, Bill E, Winkelmann G, Trautwein AX. 1987. Role of siderophores in iron storage in spores of *N. crassa* and *A. ochraceus*. *Journal of Bacteriology* **169,** 5873–5876.

Meguro R, Asano Y, Odagiri S, Li C, Iwatsuki H, Shoumura K. 2007. Nonheme-iron histochemistry for light and electron microscopy: a historical, theoretical and technical review. *Archives of Histology and Cytology* **70,** 1–19.

Moog PR, Bruggemann W. 1994. Iron reductase systems on the plant plasma-membrane—a review. *Plant and Soil* **165,** 241–260.

Morrissey J, Guerinot ML. 2009. Iron uptake and transport in plants: the good the bad and the ionome. *Chemical Reviews* **109,** 4553–4567.

Mørup S. 2011. Magnetic relaxation phenomena. In: Gütlich P**,** Bill E, Trautwein AX, eds. *Mössbauer spectroscopy and transition metal chemistry*. Berlin: Springer-Verlag, 201–234.

Müller DG, Gachon CMM, Küpper FC. 2008. Axenic clonal cultures of filamentous brown algae: initiation and maintenance. *Cahiers De Biologie Marine* **49,** 59–65.

Naito K, Suzuki M, Mito S, Hasegawa H, Imai I, Sohrin Y, Matsuin M. 2001. The pursuit of siderophore secreted by marine phytoplankton *R. ovalis*. *Analytical Science* **17,** 817–819.

Nölling J, Ishii M, Koch J, Pihl TD, Reeve JM, Thauer RK, Hedderich R. 1995. Characterization of a 45-kDa flavoprotein and evidence for a rubredoxin, two proteins that could participate in electron transport from H_2 to CO_2, in methanogenesis in *Methanobacterium autotrophicum*. *European Journal of Biochemistry* **231,** 628–638.

Paz Y, Shimoni E, Weiss M, Pick U. 2007. Effects of iron deficiency on iron binding and internalization into acidic vacuoles in *Dunaliella salina*. *Plant Physiology* **144,** 1407–1415.

Peters AF, Marie D, Scornet D, Kloareg B, Cock JM. 2004. Proposal of *Ectocarpus siliculosus* (Ectocarpales, Phaeophyceae) as a model organism for brown algal genetics and genomics. *Journal of Phycology* **40,** 1079–1088.

Ravel B. 2005. ATHENA, ARTEMIS, HEPHAESTUS: data analysis for X-ray absorption spectroscopy using IFEFFIT. *Journal of Synchrotron Radiation* **12,** 537–541.

Ravet K, Touraine B, Boucherez J, Briat JF, Gaymard F, Cellier F. 2009. Ferritins control interaction between iron homeostasis and oxidative stress in Arabidopsis. *The Plant Journal* **57,** 400–412.

Reindel S, Anemüller S, Sawaryn A, Matzanke BF. 2002. The starvation induced DNA-binding protein DpsA of the archaeon *Halobacterium salinarum* is a ferritin. *Biochimica et Biophysica Acta* **1598,** 130–136.

Robinson NJ, Procter CM, Connolly EL, Guerinot ML. 1999. A ferric-chelate reductase for iron uptake from soils. *Nature* **397,** 694–697.

Römheld V, Marschner H. 1986. Evidence for a specific uptake system for iron phytosiderophores in roots of grasses. *Plant Physiology* **80,** 175–180.

Roschzttardtz H, Conéjéro G, Curie C, Mari S. 2009. Identification of the endodermal vacuole as the iron storage compartment in the Arabidopsis embryo. *Plant Physiology* **151,** 1329–1338.

Roschzttardtz H, Conéjéro G, Curie C, Mari S. 2010. Straightforward histochemical staining of Fe by the adaptation of an old-school technique: identification of the endodermal vacuole as the site of Fe storage in Arabidopsis embryos. *Plant Signaling Behavior* **5,** 56–57.

Schünemann V, Winkler, H. 2000. Structure and dynamics of biomolecules studied by Mössbauer spectroscopy. *Reports on Progress in Physics* **63,** 263–353.

Semin BK, Davleteshina LN, Novakova AA, Kiseleve TY, Lanchinskaya VY. 2003. Accumulation of ferrous iron in *Chlamydomonas reihardtii*. Influence of CO_2 and anaerobic induction of reversible hydrogenase. *Plant Physiology* **131,** 1756–1764.

Shaked Y, Kuska AB, Morel FMM. 2005. A general kinetic model for iron acquisition by eukaryotic phytoplankton. *Limnology and Oceanography* **50,** 872–882.

Sonier MB, Weger HG. 2010. Plasma membrane ferric reductase activity of iron limited algal cells is inhibited by ferric chelators. *BioMetals* **23,** 1029–1042.

Sutak R, Slapeta J, San Roman M, Camadro JM, Lesuisse E. 2010. Nonreductive iron uptake mechanism in the marine alveolate *Chromera velia*. *Plant Physiology* **154,** 991–1000.

Trick CG, Andersen RJ, Gillam A, Harrison PJ. 1983. Prorocentrin an extracellular siderophore produced by the marine dinoflagellate *Prorocentrum minimum*. *Science* **219,** 306–308.

Trikha J, Walso GS, Lewansowski FA, Ha Y, Theil EC, Weber PC, Allewell NM. 1994. Crystallization and structural analysis of bullfrog red cell L-subunit ferritins. *Proteins* **18,** 107–118.

Wasserfallen A, Huber K, Leisinger T. 1995. Purification and structural characterization of a flavoprotein induced by iron limitation in *Methanobacterium autotrophicum* Marburg. *Journal of Bacteriology* **177,** 2436–2441.

Weger HG, Lam J, Wirtz NL, Walker CN, Treble RG. 2009. High stability ferric chelates result in decreased iron uptake by the green alga *Chlorella kessleri* owing to decreased ferric reductase activity and chelation of ferrous iron. *Botany* **87,** 922–931.

Winkler H, Meyer W, Trautwein AX, Matzanke BF. 1994. Mössbauer and EXAFS studies of bacterioferritin from *Streptomyces olivaceus*. *Hyperfine Interactions* **91,** 841–846.